Large Array Channel Capacity in the Presence of Interference

V. Vilnrotter[1] and M. Srinivasan[1]

We develop a model for a large array ground receiver system for use in deep-space communications, and analyze the resulting array channel capacity. The model includes effects of array geometry, time-dependent spacecraft orbital trajectory, point and extended interference sources, and elevation-dependent noise and tropospheric channel variations. Channel capacity is expressed as the ratio of determinants of covariance matrices characterizing source, interference, and additive noise, and then reduced to a simpler quadratic form more amenable to analysis and numerical computation. This formulation facilitates inclusion of array and channel characteristics into the model, as well as comparison of optimal, suboptimal, and equivalent single-antenna configurations on achievable throughput. Realistic examples of ground array channel capacity calculations are presented, demonstrating the impact of array geometry, planetary interference sources, and array combining algorithm design upon the achievable data throughput.

I. Introduction

One of the primary technologies for increasing downlink data rates and enabling more missions for the Deep Space Network (DSN) is the use of antenna arrays. Large arrays consisting of small to moderately sized antennas provide increased signal-to-noise ratio (SNR) gain as well as robustness and flexibility in receiving greater numbers of spacecraft signals at higher data rates. Long antenna baselines result in greater science capabilities as well as the ability to reject interference due to the resulting narrow beamwidths, especially when coupled with advanced signal processing techniques to further cancel interfering signals. In light of these benefits, it is desirable to formulate a framework for quantifying the potential gains and limitations of array reception, incorporating specific design parameters and signaling conditions. In this article, we develop an analytical framework in terms of the *array channel capacity*.

Channel capacity measures the maximum data throughput achievable on a particular channel, and is defined as the maximum mutual information between the input and output of the channel [1,2]. Array capacity for the additive white Gaussian noise (AWGN) channel has been discussed in [2,3], as well as in [4] for the DSN application. Here we follow the groundwork laid in [4], adding further detail with respect to array element geometry and layout, source signal trajectory, atmospheric effects, and interference sources. Future work may include additional factors such as primary antenna gain patterns, more complicated signal sources, hardware limitations, noise sources, and possible array combining constraints. The intent

[1] Communications Architectures and Research Section.

The research described in this publication was carried out by the Jet Propulsion Laboratory, California Institute of Technology, under a contract with the National Aeronautics and Space Administration.

is to provide an analytical basis for the ready evaluation of the extent to which changes in various array channel parameters impact achievable data throughput.

II. Modeling of the Array Channel and Signals

A. Array and Modulated Signal

Figure 1 illustrates the coordinate system and geometric parameters describing a general array layout consisting of N antennas. Referencing the antenna element positions to the coordinate system origin, the position of the ith antenna element, $1 \leq i \leq N$, is given by vector $\mathbf{a}_i = a_{x,i}\hat{\mathbf{x}} + a_{y,i}\hat{\mathbf{y}} + a_{z,i}\hat{\mathbf{z}}$, where $\hat{\mathbf{x}}$, $\hat{\mathbf{y}}$, and $\hat{\mathbf{z}}$ are unit vectors along the coordinate axes, and $a_{x,i}$, $a_{y,i}$, and $a_{z,i}$ are the projections of the vector corresponding to the ith antenna location onto the coordinate axes. The signal direction is always changing due to Earth rotation as well as source trajectory. It can be described by the unit vector $\hat{\mathbf{s}} = s_x\hat{\mathbf{x}} + s_y\hat{\mathbf{y}} + s_z\hat{\mathbf{z}}$, where the coordinate components can be conveniently expressed in terms of the source elevation and azimuth angles $(\theta_s(t), \phi_s(t))$, as illustrated in Fig. 1:

$$\begin{aligned} s_x(t) &= \cos\big(\theta_s(t)\big)\sin\big(\phi_s(t)\big) \\ s_y(t) &= \cos\big(\theta_s(t)\big)\cos\big(\phi_s(t)\big) \\ s_z(t) &= \sin\big(\theta_s(t)\big) \end{aligned} \tag{1}$$

The instantaneous time delay between the arrival of the signal plane wave at the ith and jth antennas can be determined by projecting the instantaneous antenna location vector onto the source direction vector, forming the inner product

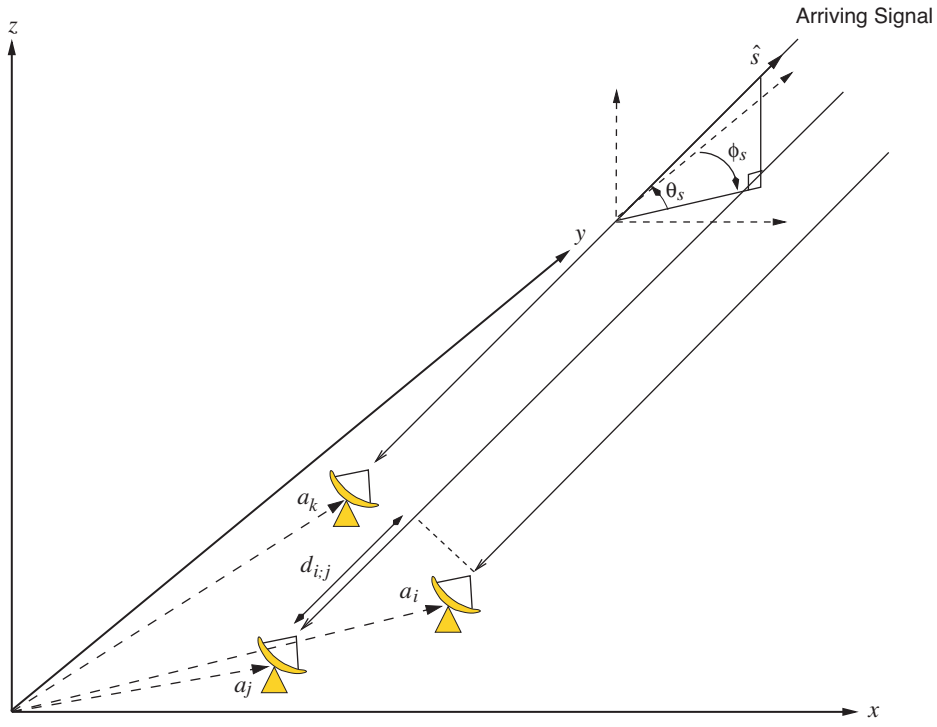

Fig. 1. Array layout.

$$\mathbf{a}_i \cdot \hat{\mathbf{s}} = a_{x,i}s_x + a_{y,i}s_y + a_{z,i}s_z$$

$$= a_{x,i}\cos\theta_s \sin\phi_s + a_{y,i}\cos\theta_s \cos\phi_s + a_{z,i}\sin\theta_s \tag{2}$$

where the time dependence has been suppressed for notational convenience. The delay difference between signals received by different antennas is directly proportional to the difference of two inner products as defined in Eq. (2). Note that if there is no height variation in the antenna phase centers, so that $a_{z,i} = 0$, then only the x and y components of the projection are non-zero; in this case, a source at zero elevation angle (at the horizon) generates the greatest possible projection in the direction of the source, hence greatest delay, since $\cos(\theta_s = 0) = 1$. A source at zenith, on the other hand, projects zero onto any of the antenna location vectors, since $\cos(\theta_s = \pi/2) = 0$.

In the context of array reception, the quantity of interest is the residual phase accumulated at each antenna due to the geometry of the array and the source, since it is the accumulated phase at each antenna that must be estimated and removed before the signal components are combined. For any array geometry, there is in general a maximal projection onto the source direction, corresponding to the antenna that first encounters the signal field; denote this antenna direction vector by the subscript zero, $\mathbf{a}_0$. All other antennas observe the signal field some time later. The phase accumulated by the signal field in traversing the distance from the first antenna to the ith antenna is proportional to the difference between the maximal inner product and the ith inner product: $2\pi(\mathbf{a}_0 - \mathbf{a}_i) \cdot \hat{\mathbf{s}}/\lambda$. Assuming that geometry-dependent delays have been removed based on predicts, we can use a narrowband array model in which the time delay results only in a phase difference between elements, so that the signal received at the ith antenna can be represented as

$$s_i(t) = \sqrt{P_{s,i}}d(t)e^{j(\omega t + 2\pi(\mathbf{a}_0 - \mathbf{a}_i)\cdot\hat{\mathbf{s}}/\lambda + \varphi_i)}$$

$$= \sqrt{P_{s,i}}d(t)e^{j2\pi\mathbf{a}_0\cdot\hat{\mathbf{s}}/\lambda}e^{j(\omega t - 2\pi\mathbf{a}_i^T\cdot\hat{\mathbf{s}}/\lambda + \varphi_i)} \tag{3}$$

Here $P_{s,i} = \gamma_i P$ is the signal power received at the ith antenna, where P is the signal power at the transmitter and γ_i is a scale factor that includes space loss, antenna gains, etc., for the ith antenna. In addition, $d(t)$ is the narrowband signal modulation, ω is the signal carrier frequency, λ is the signal wavelength, and φ_i is a fixed phase offset due to effects other than the antenna geometry. Note that since only phase differences are of interest here, we can simplify Eq. (3) by ignoring the phase term common to all antennas, yielding

$$s_i(t) = \sqrt{P_{s,i}}d(t)e^{j(\omega t - 2\pi\mathbf{a}_i\cdot\hat{\mathbf{s}}/\lambda + \varphi_i)} \tag{4}$$

If we denote the gain and phase terms for the ith antenna by $g_i(t) = \sqrt{\gamma_i}e^{j(\omega t - 2\pi\mathbf{a}_i\cdot\hat{\mathbf{s}}/\lambda + \varphi_i)}$, and let the column vector $\mathbf{G} = (g_1(t), \cdots, g_N(t))^T$, then we may write the received signal vector $\mathbf{s} = \sqrt{P}\mathbf{G}d(t)$.

This is the array geometry and signal model we will adopt in this article. Since both the carrier phasor and the signal modulation are rapidly varying terms, we continue to denote them as explicit functions of time; however, we must keep in mind that the source vector is also a time-varying quantity, and that it changes significantly on a time scale of tens of seconds to minutes over the narrow field of view of the array.

B. Additive Noise

Even if no interfering sources are present, the receiver at each antenna observes the signal in the presence of additive noise. The components of the additive noise are the cosmic background, which appears

as a spatially uniform 3-kelvin source everywhere in the sky; a frequency-dependent atmospheric contribution that varies with elevation and meteorological conditions; and thermal noise produced within the front-end electronics of the receiver itself. These noise components are assumed to be independent zero-mean white Gaussian processes; hence, a second-moment characterization provides a complete statistical description.

The variance of the total additive noise at each antenna is the sum of the component variances, some of which may be time and elevation dependent. Since the cosmic background and receiver thermal noise generally do not depend on time, we can combine them into single noise terms with variance $\sigma_{n,i}^2 = \sigma_c^2 + \sigma_{th,i}^2$ for the ith antenna. However, the contribution of the atmosphere depends on elevation and meteorological conditions; therefore, it should be denoted as a function of elevation and time: $\sigma_{atm,i}^2(\theta_s, t) = \big(\sigma_{atm,i}^2(t)\big)/(\sin\theta_s)$. This notation allows the modeling of both deterministic elevation-dependent effects and time-varying atmospheric conditions such as clouds rolling over the array.

The extension of these individual antenna models to the array can be accomplished using matrix notation. Since the noise components at each antenna are independent, we can express their noise covariance matrix as

$$\begin{aligned}\boldsymbol{\Theta}_{n,\text{total}}(\theta_s, t) &= \boldsymbol{\Theta}_n + \boldsymbol{\Theta}_{atm}(\theta_s, t) \\ &= \sigma_c^2\mathbf{I} + \begin{pmatrix} \sigma_{th,1}^2 & 0 & \dots & 0 \\ 0 & \sigma_{th,2}^2 & \dots & 0 \\ \vdots & \vdots & \ddots & \vdots \\ 0 & 0 & \dots & \sigma_{th,N}^2 \end{pmatrix} + \frac{1}{\sin(\theta_s)} \begin{pmatrix} \sigma_{atm,1}^2(t) & 0 & \dots & 0 \\ 0 & \sigma_{atm,2}^2(t) & \dots & 0 \\ \vdots & \vdots & \ddots & \vdots \\ 0 & 0 & \dots & \sigma_{atm,N}^2(t) \end{pmatrix}\end{aligned} \tag{5}$$

where $\mathbf{I}$ is the $N \times N$ identity matrix.

C. Interference

The primary sources of interference in the deep-space channel are planetary noise sources and possibly undesired modulated signals from other spacecraft. Terrestrial interference also may occur, but likely will be more sporadic in nature, unless it is due to array self-interference. Here we consider only planetary noise sources in the interference model.

A distributed interference source such as a planet may be modeled as a spatially sampled set of narrowband Gaussian point interferers [5]. For the purposes of this investigation, we model planetary noise sources as a hexagonal lattice of point sources representing spatial samples whose spacing depends upon the beamwidth of the array. The number of point sources depends upon the angular diameter of the planet. Figure 2 shows an example of a distributed interference model for a planet with an angular diameter of approximately 25 μrad, received by a 32-GHz (Ka-band) array of 100 elements with an effective diameter of approximately 800 m, resulting in an array beamwidth of about 12 μrad. With half-array-beamwidth spatial sampling (oversampled), we arrive at the hexagonal lattice shown in the figure. Each interference point source can be modeled in the same manner as the signal case developed in Section II.A, except the modulation is noise-like instead of being a structured signal. The kth interfering point source received at the ith antenna within the passband of the receiver around the signal carrier frequency, therefore, can be represented as

$$b_i^{(k)}(t) = B(t)e^{j(\omega t - 2\pi\mathbf{a}_i\cdot\hat{\mathbf{b}}^{(k)}/\lambda + \varphi_i)} \tag{6}$$

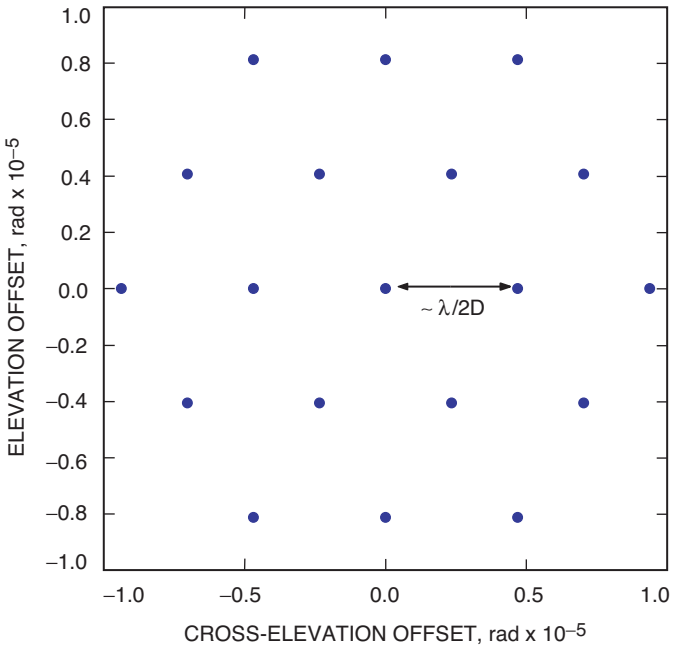

Fig. 2. Example of an oversampled distributed point source model for planetary noise, where each point is a narrowband Gaussian source.

where $B(t)$ is a complex Gaussian random process spanning the bandwidth of the receiver's predetection filter and φ_i is the nongeometric phase component. As with the signal source, the kth interferer has unit direction vector $\hat{\mathbf{b}}^{(k)}(t) = b_x^{(k)}(t)\hat{\mathbf{x}} + b_y^{(k)}(t)\hat{\mathbf{y}} + b_z^{(k)}(t)\hat{\mathbf{z}}$, with components

$$b_x^{(k)}(t) = \cos\left(\theta_b^{(k)}(t)\right)\sin\left(\phi_b^{(k)}(t)\right)$$

$$b_y^{(k)}(t) = \cos\left(\theta_b^{(k)}(t)\right)\cos\left(\phi_b^{(k)}(t)\right)$$

$$b_z^{(k)}(t) = \sin\left(\theta_b^{(k)}(t)\right)$$

where $\theta_b^{(k)}(t)$ and $\phi_b^{(k)}(t)$ are the elevation and azimuth angles of the kth interfering signal. Note that the remaining temporal variation in Eq. (6) is slow, being the result of changing geometry, whereas the variation in $B(t)$ is more rapid since the noise-like modulation is broadband. Assuming that delay differences between antennas have been removed to an accuracy commensurate with the receiver bandwidth, we can model the background interference as a white process with variance $E\left[|B(t)|^2\right] = 2\sigma_b^2$. The covariance matrix of the kth interferer has entries of the form

$$\mathbf{\Theta}_b^{(k)}(i,l) = E\left[b_i^{(k)}(t)b_l^{(k)*}(t)\right] = 2\sigma_b^2 e^{j2\pi(\mathbf{a}_l - \mathbf{a}_i)\cdot\hat{\mathbf{b}}^{(k)}/\lambda + j(\varphi_i - \varphi_l)} \tag{7}$$

If there is a cluster of interferers, or if a distributed interferer is modeled as a set of point samples, the covariance entries for each point can be determined as in Eq. (7). With the further assumption that each interferer generates independent noise-like processes (this is the case if the coefficients of an extended

source were obtained via a Karhounen–Loeve expansion, as assumed here), the covariance entries of the sum of interferers can be obtained as the sum of the individual covariance entries, $\mathbf{\Theta}_b = \sum_{k=1}^{K} \mathbf{\Theta}_b^{(k)}$.

D. Atmospheric Effects

As signals pass through the atmosphere, they are affected in two ways. The signal power is attenuated by an amount proportional to the thickness of the atmosphere, and the phase is perturbed by the turbulent medium. The additional Gaussian noise that the atmosphere contributes to the received signal was discussed in Section II.B.

In evaluating the impact of these effects, we can model the atmospheric attenuation and phase either as deterministic quantities or as random processes. In this article, we primarily consider the deterministic case. Assume that each antenna element sees a column of atmosphere independently of the other antennas. This model is valid for antennas of 10-m diameter or larger, spaced sufficiently far apart to avoid shadowing at low elevations. Then we can define diagonal atmospheric attenuation and phase matrices $\mathbf{H}_{atm}$ and $\mathbf{\Psi}_{atm}$, which are elevation and time dependent:

$$\mathbf{H}_{atm} = \begin{pmatrix} h_1(\theta,t) & 0 & \dots & 0 \\ 0 & h_2(\theta,t) & \dots & 0 \\ \vdots & \vdots & \ddots & \vdots \\ 0 & 0 & \dots & h_N(\theta,t) \end{pmatrix} \tag{8}$$

and

$$\mathbf{\Psi}_{atm} = \begin{pmatrix} \psi_1(\theta,t) & 0 & \dots & 0 \\ 0 & \psi_2(\theta,t) & \dots & 0 \\ \vdots & \vdots & \ddots & \vdots \\ 0 & 0 & \dots & \psi_N(\theta,t) \end{pmatrix} \tag{9}$$

We can now write the received signal at the ith antenna as

$$\tilde{s}_i(t) = h_i(\theta_s,t)\sqrt{P_{s,i}}d(t)e^{j(\omega t - 2\pi \mathbf{a}_i \cdot \hat{\mathbf{s}}/\lambda + \varphi_i + \psi_i(\theta_s,t))}$$

and the received interference at the ith antenna from the kth interferer as

$$\tilde{b}_i^{(k)}(t) = h_i(\theta_b,t)B(t)e^{j\left(\omega t - 2\pi \mathbf{a}_i \cdot \hat{\mathbf{b}}^{(k)}/\lambda + \varphi_i + \psi_i(\theta_b,t)\right)}$$

where ψ_i is the additional phase accumulated in propagating through the atmosphere, and φ_i represents residual instrumental phase effects, as before. The "$\sim$" notation indicates sensitivity to atmospheric phase variations over the array elements. Recalling that for diagonal matrices,

$$e^{j\mathbf{\Psi}} = \mathbf{I} + j\mathbf{\Psi} - \mathbf{\Psi}^2/2 + \ldots = \begin{pmatrix} e^{j\psi_1} & 0 & \dots & 0 \\ 0 & e^{j\psi_2} & \dots & 0 \\ \vdots & \vdots & \ddots & \vdots \\ 0 & 0 & \dots & e^{j\psi_N} \end{pmatrix}$$

we can separately incorporate the amplitude and phase effects of the atmosphere on the observed signal and interference column vectors as

$$\tilde{\mathbf{s}} = \mathbf{H}_{atm} e^{j\mathbf{\Psi}_{atm}} \mathbf{s} = \mathbf{H}_{atm} e^{j\mathbf{\Psi}_{atm}} \mathbf{G}\sqrt{P} d(t)$$

and

$$\tilde{\mathbf{b}}^{(k)} = \mathbf{H}_{atm} e^{j\mathbf{\Psi}_{atm}} \mathbf{b}^{(k)}$$

For ease of notation, we have used the same atmospheric amplitude and phase matrices for both signal and interference sources, implying that the signals are subjected to the same atmospheric effects. This approximation is valid for small source-interference angles.

The signal outer product and interference covariance matrices may now be written in the form

$$\begin{aligned}
\tilde{\mathbf{s}}\tilde{\mathbf{s}}^{*T} &= \mathbf{H}_{atm} e^{j\mathbf{\Psi}_{atm}} \mathbf{s}\mathbf{s}^{*T} e^{-j\mathbf{\Psi}_{atm}} \mathbf{H}_{atm}^{*T} \\
&= P|d(t)|^2 \mathbf{H}_{atm} e^{j\mathbf{\Psi}_{atm}} \mathbf{G}\mathbf{G}^{*T} e^{-j\mathbf{\Psi}_{atm}} \mathbf{H}_{atm}^{*T} \\
&= P|d(t)|^2 \mathbf{H}\mathbf{G}\mathbf{G}^{*T}\mathbf{H}^{*T} \qquad (10)
\end{aligned}$$

and

$$\begin{aligned}
\tilde{\mathbf{\Theta}}_b^{(k)} = E\left[\tilde{\mathbf{b}}^{(k)}\tilde{\mathbf{b}}^{(k)*T}\right] &= E\left[\mathbf{H}_{atm} e^{j\mathbf{\Psi}_{atm}} \mathbf{b}^{(k)}\mathbf{b}^{(k)*T} e^{-j\mathbf{\Psi}_{atm}} \mathbf{H}_{atm}^{*T}\right] \\
&= \mathbf{H}\mathbf{\Theta}_b^{(k)}\mathbf{H}^{*T} \qquad (11)
\end{aligned}$$

where we define the complex channel matrix $\mathbf{H} \equiv \mathbf{H}_{atm} e^{j\mathbf{\Psi}_{atm}}$. Having modeled all significant noise sources, the general form of the noise-plus-interference covariance matrix may be expressed as

$$\tilde{\mathbf{\Theta}}_z = \mathbf{\Theta}_n + \mathbf{\Theta}_{atm}(\theta, t) + \sum_{k=1}^{K} \tilde{\mathbf{\Theta}}_b^{(k)} \qquad (12)$$

where (θ, t) denotes variation with elevation and time. Although not stated explicitly, we note that both elevation and time dependence in the signal and interference terms are incorporated into the covariance matrix through the atmospheric attenuation and atmospheric phase matrices.

III. Array Capacity

The capacity of an array for Gaussian channels has been derived in [4], where the problem was formulated as a single-source, multiple input–multiple output channel. We now generalize the array capacity derivation for the channel model shown in Fig. 3, which includes array geometry, atmospheric effects, and directional Gaussian interference. This model applies to a single spacecraft transmitter broadcasting to Earth, where a multitude of receivers observe the same message, but with generally different delays due to geometry and atmospheric effects. We assume that large delay variations have been compensated for, leaving only small residual delays that can be adequately modeled as a phase shift on the modulated carrier. In Fig. 3, the source X undergoes different gains and geometric phase offsets (denoted

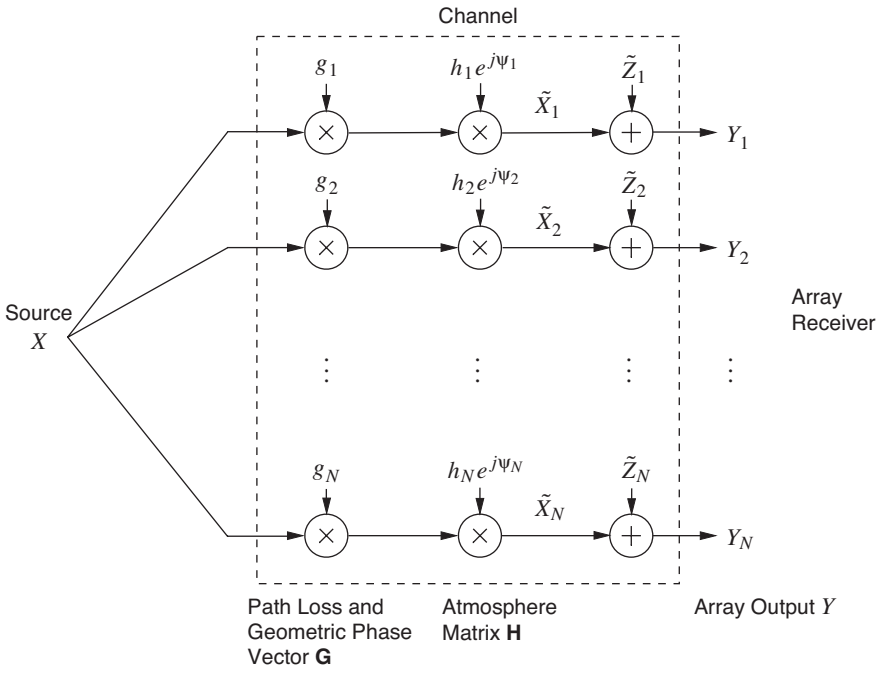

Fig. 3. Array channel model.

by the vector $\mathbf{G}$, as in Section II.A) at each of the array elements. The signal also is subjected to atmospheric effects as represented by the matrix $\mathbf{H}$. The vector of signals arriving at the N antennas then may be denoted by $\tilde{\mathbf{X}} = \mathbf{HG}X$. The additive noise vector $\tilde{\mathbf{Z}}$ consists of Gaussian interference signals subject to geometric phase offsets and atmosphere as well as Gaussian, cosmic, and receiver thermal noise, having covariance matrix $\tilde{\mathbf{\Theta}}_Z$ given in Eq. (12). The received array vector is then $\mathbf{Y} = \tilde{\mathbf{X}} + \tilde{\mathbf{Z}}$.

The array capacity C_{array} is defined as the maximum mutual information between the single source X and the array output observables $\mathbf{Y} = (Y_1, Y_2, \cdots, Y_N)^T$ over all possible distributions of source symbols, subject to the power constraint $E(|X|^2) = P$. The capacity can be expressed as a maximization of the difference between the entropy of the vector observable $H(\mathbf{Y})$ and the entropy of the additive noise $H(\mathbf{Z})$, obtained via the following derivation:

$$
\begin{aligned}
C_{\text{array}} &= \max_p I(\mathbf{Y}; X) \\
&= \max_p \left\{ H(\mathbf{Y}) - H(\mathbf{Y}|X) \right\} \\
&= \max_p \left\{ H(\mathbf{Y}) - H(\mathbf{HG}X + \tilde{\mathbf{Z}}|X) \right\} \\
&= \max_p \left\{ H(\mathbf{Y}) - H(\tilde{\mathbf{Z}}) \right\} \qquad (13) \\
&= \left(\max_p H(\mathbf{Y}) \right) - H(\tilde{\mathbf{Z}}) \qquad (14)
\end{aligned}
$$

where $H(\mathbf{Y}|X)$ is the conditional entropy of the vector $\mathbf{Y}$ averaged over the source alphabet X, and p is the probability distribution of the source symbols. Equation (13) follows because $\mathbf{G}$ and $\mathbf{H}$ are known,

and $\tilde{\mathbf{Z}}$ is independent of X. The power constraint on X along with the known quantities $\mathbf{G}$ and $\mathbf{H}$ determine the covariance matrix of $\mathbf{Y}$:

$$\begin{aligned}\boldsymbol{\Theta}_Y = E(\mathbf{Y}\mathbf{Y}^{*T}) &= E\left((\mathbf{HG}X + \tilde{\mathbf{Z}})(\mathbf{HG}X + \tilde{\mathbf{Z}})^{*T}\right) \\ &= E(|X|^2)\mathbf{HG}(\mathbf{GH})^{*T} + E(\tilde{\mathbf{Z}}\tilde{\mathbf{Z}}^{*T}) \\ &= P\mathbf{HG}(\mathbf{GH})^{*T} + \tilde{\boldsymbol{\Theta}}_Z \\ &= \tilde{\boldsymbol{\Theta}}_X + \tilde{\boldsymbol{\Theta}}_Z \end{aligned} \tag{15}$$

where we have defined $\tilde{\boldsymbol{\Theta}}_X = E(\tilde{\mathbf{X}}\tilde{\mathbf{X}}^{*T}) = P\mathbf{HG}(\mathbf{GH})^{*T}$.

Theorem 9.6.5 in [2] states that, when the covariance matrix $\boldsymbol{\Theta}_Y$ is fixed, the distribution that maximizes $H(\mathbf{Y})$ is zero-mean Gaussian, and its entropy is

$$H(\mathbf{Y}) = \frac{1}{2}\log_2\left[(2\pi e)^N|\boldsymbol{\Theta}_Y|\right] = \frac{1}{2}\log_2\left[(2\pi e)^N|\tilde{\boldsymbol{\Theta}}_X + \tilde{\boldsymbol{\Theta}}_Z|\right] \tag{16}$$

where $|\Theta_y|$ denotes the determinant of Θ_y, etc. As $\tilde{\mathbf{Z}}$ is the sum of several zero-mean Gaussian processes (some of which are scaled by constant factors), it is also zero-mean Gaussian. From Theorem 9.4.1 in [2], its entropy is

$$H(\tilde{\mathbf{Z}}) = \frac{1}{2}\log_2\left[(2\pi e)^N|\tilde{\boldsymbol{\Theta}}_Z|\right] \tag{17}$$

Substituting Eqs. (16) and (17) into Eq. (14), we obtain

$$\begin{aligned} C_{\text{array}} &= \frac{1}{2}\log_2\left[(2\pi e)^N|\tilde{\boldsymbol{\Theta}}_X + \tilde{\boldsymbol{\Theta}}_Z|\right] - \frac{1}{2}\log_2\left[(2\pi e)^N|\tilde{\boldsymbol{\Theta}}_Z|\right] \\ &= \frac{1}{2}\log_2\left(\frac{|\tilde{\boldsymbol{\Theta}}_X + \tilde{\boldsymbol{\Theta}}_Z|}{|\tilde{\boldsymbol{\Theta}}_Z|}\right) \\ &= \frac{1}{2}\log_2\left(\frac{|P\mathbf{HG}(\mathbf{GH})^{*T} + \tilde{\boldsymbol{\Theta}}_Z|}{|\tilde{\boldsymbol{\Theta}}_Z|}\right) \end{aligned} \tag{18}$$

Note that the covariance matrix of the modified source vector, $\tilde{\boldsymbol{\Theta}}_X$, is equivalent to the signal outer product as given in Eq. (10), assuming that $|d(t)|^2 = 1$, i.e., $\tilde{\boldsymbol{\Theta}}_X = E\left[\tilde{\mathbf{X}}\tilde{\mathbf{X}}^{*T}\right] = \tilde{\mathbf{s}}\tilde{\mathbf{s}}^{*T}$. We can thus write

$$C_{\text{array}} = \frac{1}{2}\log_2\left(\frac{|\tilde{\boldsymbol{\Theta}}_X + \tilde{\boldsymbol{\Theta}}_Z|}{|\tilde{\boldsymbol{\Theta}}_Z|}\right) = \frac{1}{2}\log_2\left(\frac{|\tilde{\mathbf{s}}\tilde{\mathbf{s}}^{*T} + \tilde{\boldsymbol{\Theta}}_Z|}{|\tilde{\boldsymbol{\Theta}}_Z|}\right) = \frac{1}{2}\log_2\left(1 + \tilde{\mathbf{s}}^{*T}\tilde{\boldsymbol{\Theta}}_Z^{-1}\tilde{\mathbf{s}}\right) \tag{19}$$

The last expression in Eq. (19) containing the quadratic form is the result of applying Corollary A.3.1 of [6]. The quadratic form in Eq. (19) is a generalized SNR that applies to correlated as well as uncorrelated noise.

In order to achieve the performance gain that motivates use of an antenna array, the antenna output observables $\mathbf{Y}$ must be combined. Let us consider a receiver structure that uses a linear combination of the array observables, i.e., $\mathbf{w}^{*T}\mathbf{Y}$, where $\mathbf{w}$ is a weight vector. The maximum combined SNR is achieved when the weights are given by the Wiener solution $\mathbf{w}^* = \tilde{\boldsymbol{\Theta}}_Z^{-1}\tilde{\mathbf{s}}$, which also happens to yield the quadratic form obtained in Eq. (19):

$$\mathrm{SNR} \equiv \frac{\mathbf{w^T}\tilde{\mathbf{s}}\tilde{\mathbf{s}}^{*\mathbf{T}}\mathbf{w}^*}{\mathbf{w^T}\tilde{\boldsymbol{\Theta}}_{\mathbf{Z}}\mathbf{w}^*} = \frac{\tilde{\mathbf{s}}^{*T}\tilde{\boldsymbol{\Theta}}_Z^{-1}\tilde{\mathbf{s}}\tilde{\mathbf{s}}^{*T}\tilde{\boldsymbol{\Theta}}_Z^{-1}\tilde{\mathbf{s}}}{\tilde{\mathbf{s}}^{*T}\left[\tilde{\boldsymbol{\Theta}}_Z^{-1}\tilde{\boldsymbol{\Theta}}_Z\right]\tilde{\boldsymbol{\Theta}}_Z^{-1}\tilde{\mathbf{s}}} = \tilde{\mathbf{s}}^{*T}\tilde{\boldsymbol{\Theta}}_Z^{-1}\tilde{\mathbf{s}} \tag{20}$$

This implies that the operation consisting of multiplying each array output with the optimum Wiener weight and summing, thus converting the vector channel into a single channel, yields the same capacity for the single channel as for the array channel. However, this conclusion holds only for optimum weights; any error in estimating the optimum weights necessarily decreases the SNR in Eq. (20), causing a decrease in array capacity.

For the special case of a diagonal covariance matrix with components $\sigma_{atm,i}^2/\sin(\theta) + \sigma_{n,i}^2$ along the diagonal (due to elevation-dependent uncorrelated atmospheric noise plus electronics and cosmic noise contribution as defined in Section II.B), the quadratic form can be expressed as

$$\tilde{\mathbf{s}}^{*T}\tilde{\boldsymbol{\Theta}}_Z^{-1}\tilde{\mathbf{s}} = \sum_{i=1}^{N} P_{s,i}|h_i|^2 / \left(\sigma_{atm,i}^2/\sin(\theta) + \sigma_{n,i}^2\right) = \sum_{i=1}^{N} \mathrm{SNR}_i$$

where we recognize the terms inside the summation as the effective signal-to-noise ratio observed by the ith antenna, SNR_i, incorporating elevation-dependent atmospheric noise and signal attenuation, as well as independent thermal noise, but not spatially resolved background interference. The capacity expression now depends only on the sum of the individual antenna signal-to-noise ratios:

$$C_{\mathrm{array}} = \frac{1}{2}\log_2\left(1 + \tilde{\mathbf{s}}^{*T}\tilde{\boldsymbol{\Theta}}_Z^{-1}\tilde{\mathbf{s}}\right) = \frac{1}{2}\log_2\left(1 + \sum_{i=1}^{N} P_{s,i}|h_i|^2/\left(\sigma_{atm,i}^2/\sin(\theta) + \sigma_{n,i}^2\right)\right)$$

$$= \frac{1}{2}\log_2\left(1 + \sum_{i=1}^{N} \mathrm{SNR}_i\right)$$

In the simple example where background interference is negligible, array capacity can be computed directly in terms of the atmospheric attenuation, atmospheric noise, and electronics noise variance.

Note that in the preceding analysis we assumed that the phase could be measured with sufficient accuracy to justify treating it as a deterministic quantity. This would typically be the case when high-data-rate telemetry is received, ensuring high SNR in a relatively long phase measurement since a minimum symbol SNR must be maintained for the communications channel. Alternately, the time-varying phase may appear as a rapidly fluctuating quantity that cannot be measured accurately, in which case it might be more appropriate to treat it as a random quantity. This may occur with very low data-rate telemetry, where the number of symbols per phase correlation time is not sufficient to ensure accurate measurement

of the fluctuating phase process. The random process model, however, requires a re-derivation of the capacity expression and will not be addressed here.

IV. Numerical Results

In this section, we present some examples of large array capacity calculations using the various models developed in the previous sections. Note that in these calculations the antenna elements are assumed to be isotropic, and the signal sources are taken to be Gaussian. Use of a more realistic channel, such as binary phase-shift keying (BPSK) with additive Gaussian noise, will result in a reduction in capacity relative to the Gaussian input channel. In addition, we do not model atmospheric attenuation of the signal in these numerical results. Future work may incorporate more complicated atmospheric modeling as well as directional antenna gains and non-Gaussian signal sources.

In Fig. 4 we show a simple example of the effect of interference on capacity. We assume a uniformly spaced two-dimensional (square) Ka-band array with a fixed per-element symbol SNR of −30 dB and plot capacity as a function of increasing numbers of antenna elements, with and without a Gaussian point-source interferer 10 dB higher in power than the desired signal, spaced 10 μrad away from the signal. With fixed-element spacing, the drop in capacity from interference becomes smaller as the number of antennas grows. This is due to the fact that, as the effective array diameter increases, the array beamwidth becomes narrower, allowing better discrimination between signal and interference. Note that the apparent convergence of the two curves when there is just one antenna is due to the fact that the SNR per antenna element is so low and the interferer, whose power is a fixed multiple of the signal power, simply is dominated by the thermal noise and does not affect the capacity in a significant manner.

The effect of array layout is also of interest, as it is possible to optimize array capacity as a function of antenna position [3]. For example, in Fig. 5 we show a regular (uniformly spaced) 100-element array as well as an irregular array layout that has been designed for the Microwave Array Project [7]. Here, the

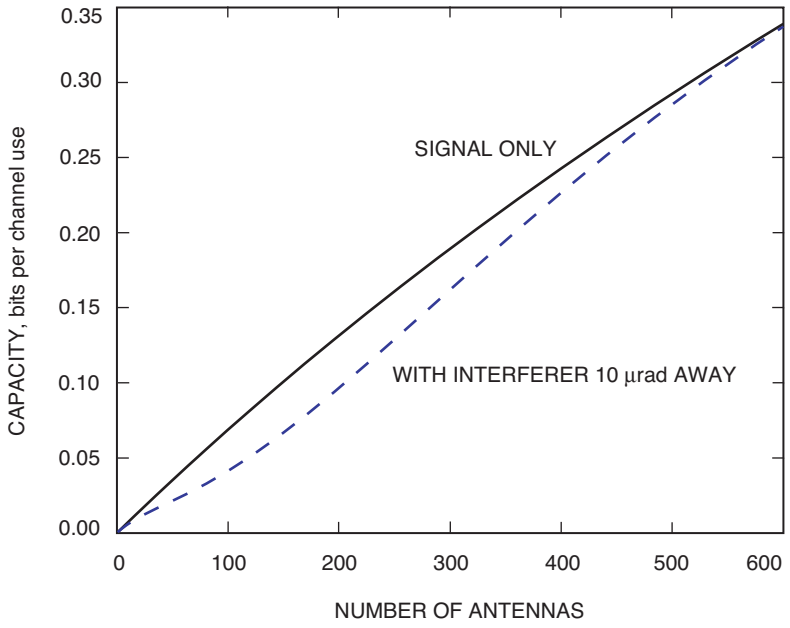

Fig. 4. Capacity as a function of the number of elements with the point interferer 10 μrad from the desired signal, a regular two-dimensional array with 50-m element separation, –30 dB per element SNR, and –10 dB per element signal-to-interference ratio.

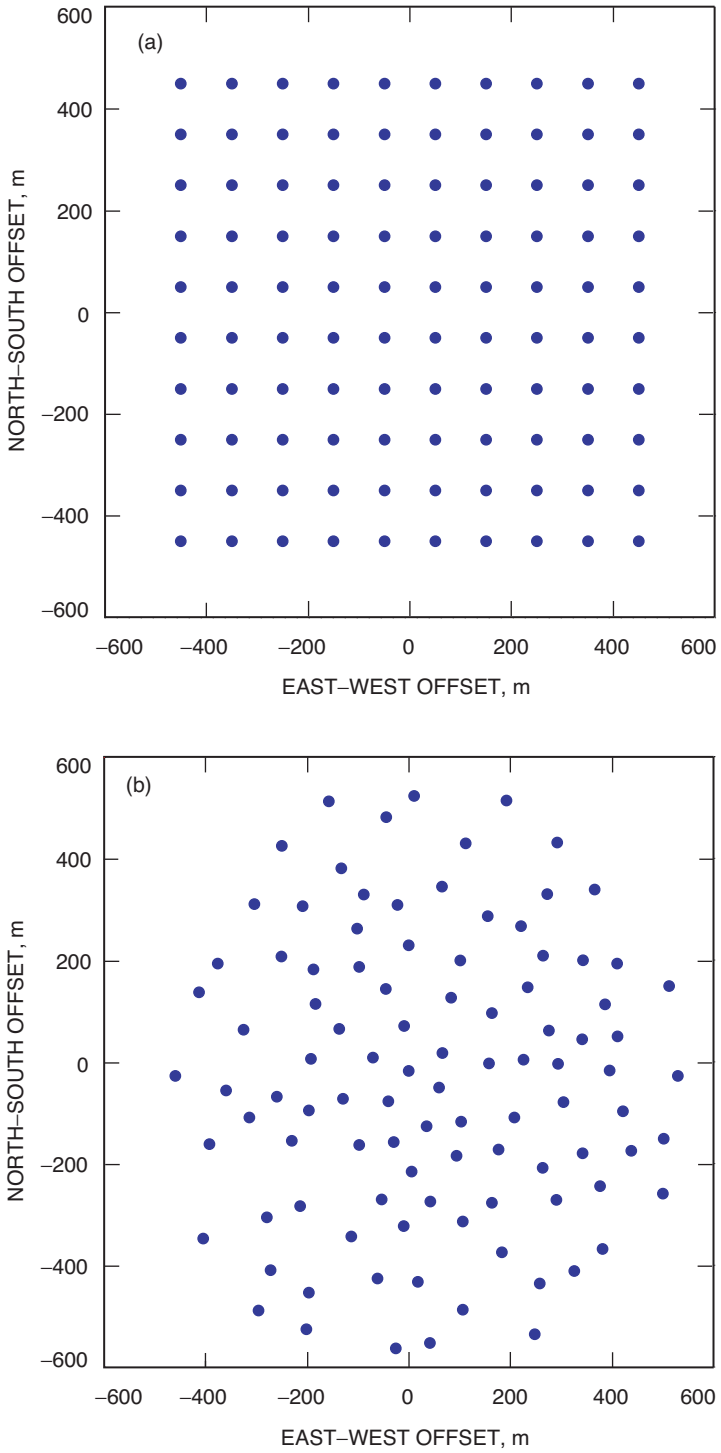

Fig. 5. Array layouts for (a) regular and (b) irregular 100-element antenna arrays.

desired signal source is placed at azimuth angle $\phi_s = \pi/3$ and elevation angle $\theta_s = \pi/4$. A Gaussian point interference source equal in power to the desired signal is placed at the same azimuth angle, $\phi_b = \phi_s$, while its elevation angle θ_b is varied in its spacing from the desired signal. Figure 6 shows the capacity at Ka-band as a function of the signal-interference separation in elevation angle for the regular and randomized array layouts of Fig. 5, assuming −5 dB ideal combined symbol SNR. We see that when the separation is less than an array beamwidth (approximately 10 μrad at Ka-band), the capacity is significantly reduced from its maximum value of approximately 0.2 bits per channel use. The fact that the regular array has slightly higher capacity in this region is due to imprecision in scaling the diameter of the irregular array in order to match its beamwidth to that of the regular array. Note that the regular array suffers additional drops in capacity at separations of 1, 6, and 30 mrad as well. This is due to grating lobes in the array beam pattern from the uniform array spacing. The randomized array does not suffer from this defect, having been designed to minimize grating lobes.

While it is clear that the irregular spacing of antenna elements will prevent large losses from interference admitted though grating lobes, it is less clear how various randomized arrays compare with each other. In Fig. 7 we show three different irregular array layouts, each comprising 50 Ka-band antenna elements. The first set of antennas is selected more or less uniformly from the Microwave Array layout shown in Fig. 5; the second set is chosen from the "eastern" antennas; and the third set is chosen from the "northern" antennas. A sample spacecraft trajectory in a 5000-km orbit around Mars is assumed (shown in Fig. 8), and capacity is calculated as a function of time over this track for a spacecraft signal with 2-dB ideal combined symbol SNR over a set of 50 elements. Mars is assumed to have an angular diameter of 30 μrad and is modeled as a cluster of 37 Gaussian point sources whose total summed power is nominally 6.9 dB lower than the signal power. In addition, elevation-angle-dependent atmospheric noise 3 dB below the thermal noise power is included. Atmospheric attenuation of the signal is not assumed here, and a deterministic assumption is made for the atmospheric phase process. Figure 9 shows the resulting capacity for the three different antenna sets. There are several features of note in these plots. The overall increase and decrease in capacity over the track is due to the spacecraft elevation profile as shown in Fig. 8 and the atmospheric noise that increases as elevation angle decreases. The periodic dips in the capacity curves are due to the changes in separation between the signal and the planetary interferer as the spacecraft orbits around Mars. Finally, we observe that there are differences between the capacity curves for the

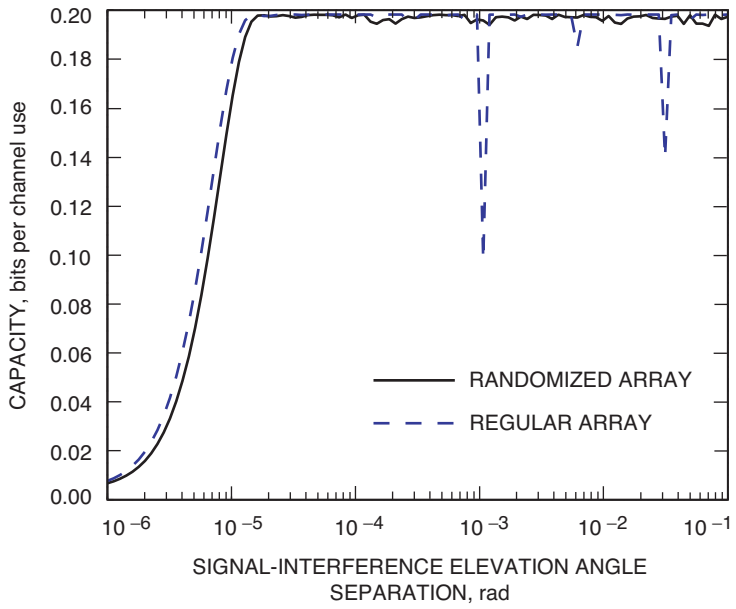

Fig. 6. Comparison of capacity for regular and irregular arrays of 100 elements at –5 dB combined symbol SNR.

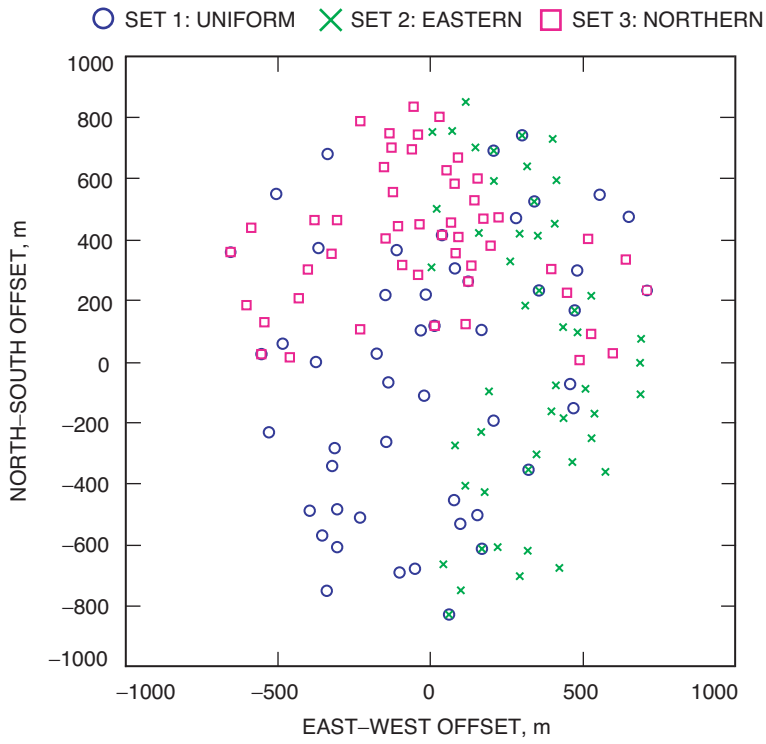

Fig. 7. Three different irregular 50-element antenna arrays.

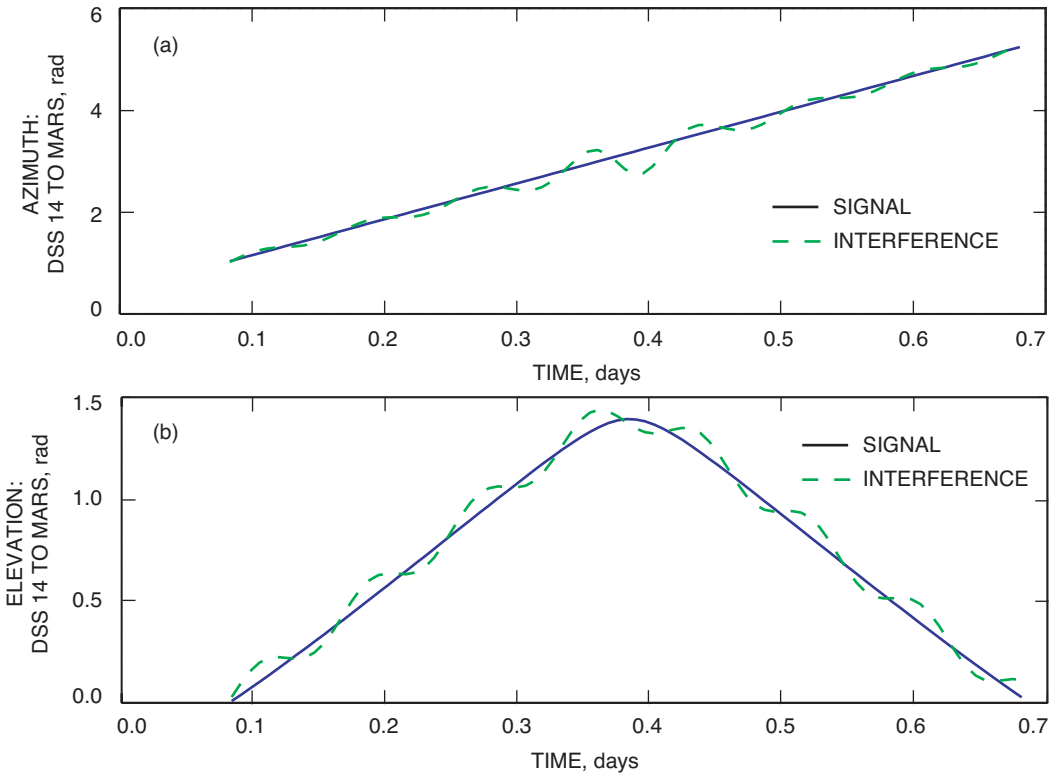

Fig. 8. Sample spacecraft profiles in a 5000-km orbit around Mars at maximum range from Earth: (a) azimuth angle and (b) elevation angle. (Mars orbit exaggerated.)

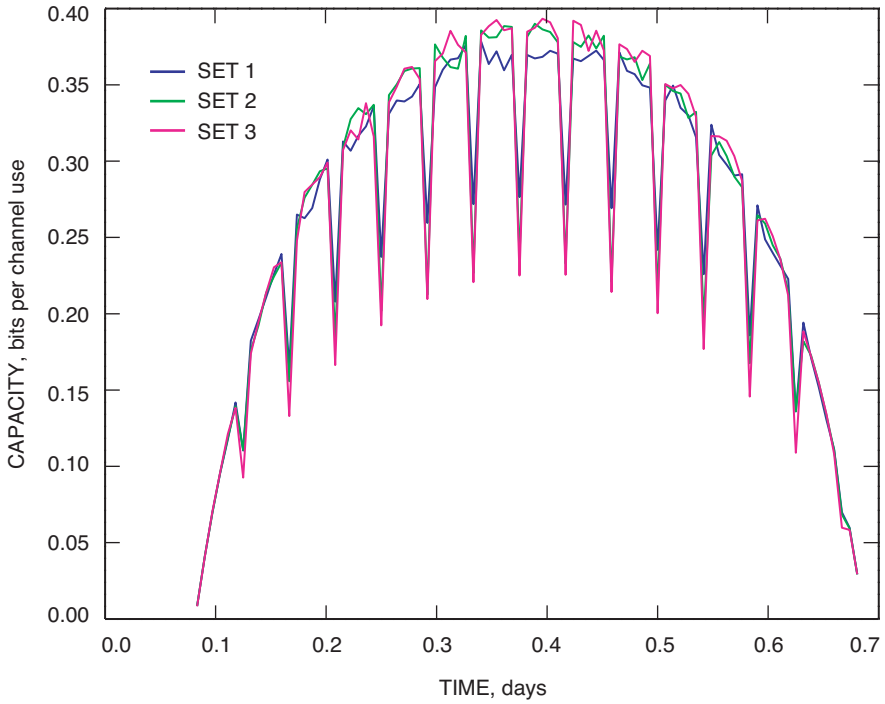

Fig. 9. Capacity curves for the three arrays shown in Fig. 7 (max snr = 2.00 dB).

three sets, with the uniform set 1 performing better when Mars is closest to the spacecraft and sets 2 and 3 performing better than set 1 when the spacecraft is near zenith and is maximally separated from Mars. These effects are due to the quality of the beam formed by the various arrays and demonstrate that the selection of antenna elements to support a particular spacecraft track can affect the achievable data throughput to some degree. We conclude that capacity is a useful metric that should be considered when performing array partitioning for mission support.

Using the same spacecraft orbit as in the previous example, we now consider the effect of various types of processing upon capacity in Fig. 10. Using the 100-element Ka-band array shown in Fig. 5(b), we plot capacity as a function of time, with Mars at maximum and intermediate range. The ideal combined symbol SNR is set to 2 dB here, which corresponds to an average signal-to-interference ratio of approximately -5 dB in the worst case with Mars at intermediate range. In the maximum range case, the angular diameter of Mars as seen from Earth is about 15 μrad, resulting in an interference model consisting of 2 points. In the intermediate range case, it is about 45 μrad and is modeled using a cluster of 37 Gaussian point sources. We consider three types of signal processing here. The first is optimal array processing, which maximizes combined output SNR and hence maximizes capacity. Optimal processing for the Gaussian channel uses the Wiener array combining weights as explained in Section III. The second type of array processing is a suboptimal method in which the steering vector for the desired signal is used to point the array elements in the proper direction. Third, we include the capacity obtained from using a single antenna with collecting area equivalent to that of the entire array. Here we assumed use of 100 12-m antennas, so the equivalent single aperture area is approximately 10,000 square meters. The single large antenna performance was actually calculated by using the 100 antennas clustered together to have the appropriate diameter, in order to actually achieve the beamforming, since the simulations model only isotropic beam patterns. As in Fig. 9, we see that the capacity oscillates with the spacecraft–Mars separation, but that the dips in capacity are much greater when Mars is at intermediate range, due to the higher interference power in that case. Note that the peak capacity values with optimal array processing are similar in the two plots, demonstrating that this array has equal interference rejection capability at

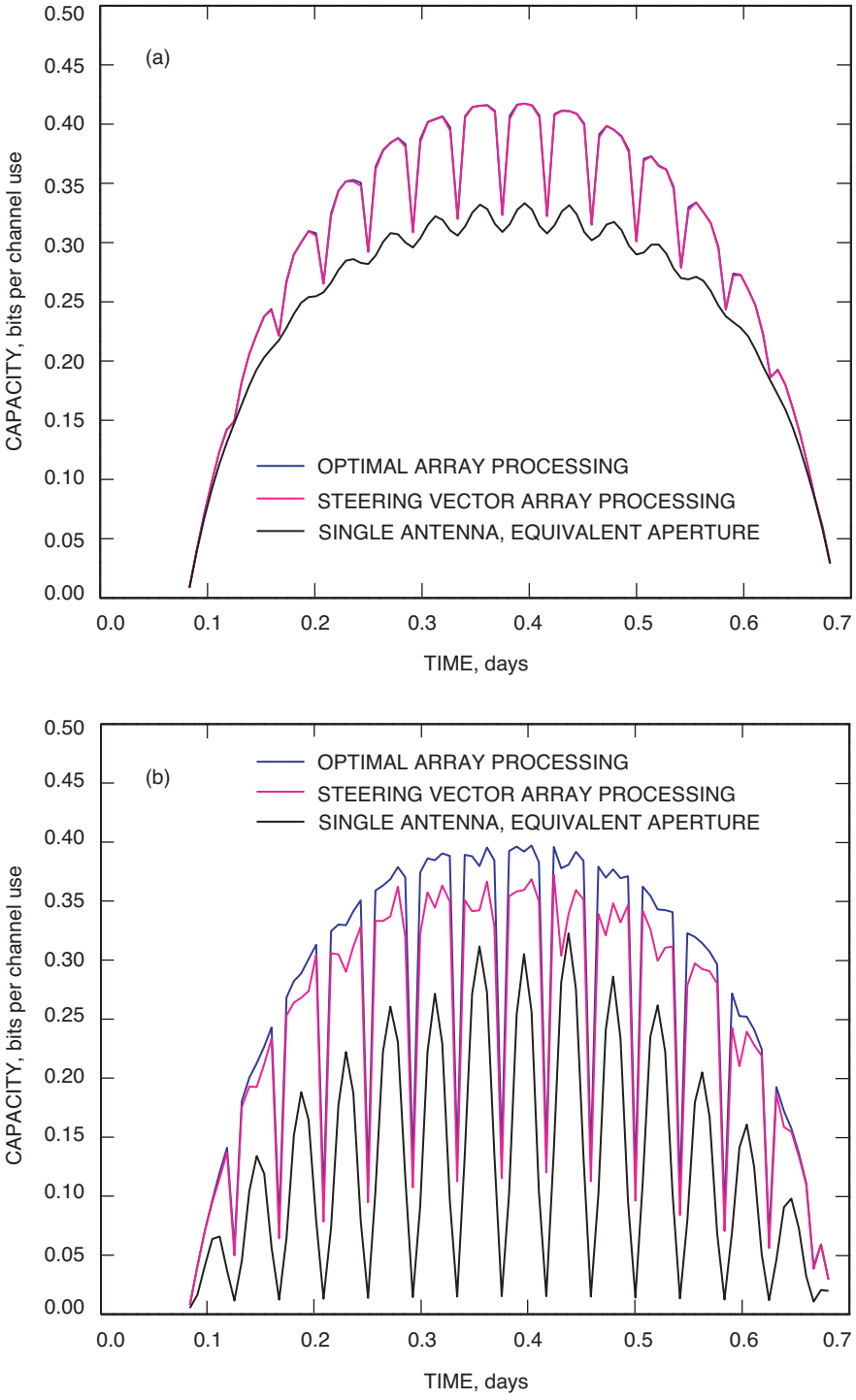

Fig. 10. Capacity of an array with optimal processing, steering vector processing, and a single antenna of equivalent aperture size (max SNR = 2.00 dB)**: (a) Mars at maximum range and (b) Mars at intermediate range.**

those points for both Mars distances. The suboptimal steering vector array combining method performs very closely to the optimal array processing when Mars is at maximum range, but can be significantly worse when Mars is closer, since it does not perform the interference nulling that is necessary with the larger extent of interference in that case. Finally, we observe the array processing gain relative to performance of a single antenna equal in aperture area to the sum of the array elements. Note that the single antenna has the same received SNR as the array but lacks the resolution and degrees of freedom that allow the array to perform beamforming and interference rejection. Hence, we see that, for this example scenario, optimal array processing provides 1.5 to 10 times improvement over performance with a single antenna of equal collecting area.

Our last two plots relate to the spatial modeling of the atmospheric phase values. In Fig. 11(a), we plot capacity for a linear array of 50 elements at Ka-band, with the desired signal at a 60-deg elevation angle and an ideal combined symbol SNR of 0 dB, and with an equal-power Gaussian interferer spaced 1 μrad away. The spacing between adjacent antennas is varied from 50 to 500 m, and the corresponding capacity is calculated while incorporating atmospheric phase values. In [8], spatial and temporal correlation properties of the tropospheric phase process were derived for the case of the large array, based upon models developed in [9,10]. Denoting the phase components associated with the signal observed by each antenna as $\{\xi_i, 1 \leq i \leq N\}$, we model them as zero-mean Gaussian random variables with covariance matrix $\mathbf{R}_\xi$. As discussed in some detail in [8], the spatial correlation of the carrier phase between two antennas is derived from the phase structure function $\sigma^2_{\Delta\xi}(d_{i,k})$ [plotted in Fig. 11(b)], which is a function of the carrier frequency and direction of arrival, the distance $d_{i,k}$ between antennas, and turbulence parameters such as the height of the troposphere, the turbulence strength, and the outer scale of turbulence. We generate a spatially correlated set of phases assuming a turbulence constant of 2.4×10^{-7} m$^{-1/3}$, a tropospheric height of 1000 m, and a turbulence outer scale of 3000 km, as in [9]. In Fig. 11, the blue curve shows the capacity of the linear array as a function of element spacing without an atmospheric phase process. As expected, the capacity increases with element spacing due to the resulting narrower beamwidth up to the point that the interferer is more or less completely rejected, after which the capacity remains constant. The magenta curves show the capacity when the atmospheric phase process is included. The discrete points represent the instantaneous capacity obtained given a particular instance of atmospheric phase values, while the solid curve is the ensemble average capacity. We observe here that the incorporation of atmospheric phase correlation does not appear to alter the capacity significantly from the no-atmosphere case, as one would expect when assuming that the phases can be tracked and treated as known quantities.

V. Conclusions

The channel capacity of an array receiver in a Gaussian channel was investigated. An analytical framework was developed to incorporate the effects of array geometry, interference, and atmospheric attenuation and phase into capacity calculations. Numerical results were presented showing the impact of array layout configuration, spacecraft orbit, and planetary interference upon throughput. Of particular significance was the demonstration of distinct improvement in achievable throughput when using the optimal Wiener array combining weights in the presence of interference rather than combining elements based upon use of the signal steering vector.

Acknowledgments

The authors would like to thank Kenneth Andrews for his careful review and valuable suggestions, and Sam Dolinar and Bruce Moision for several insightful discussions on this subject.

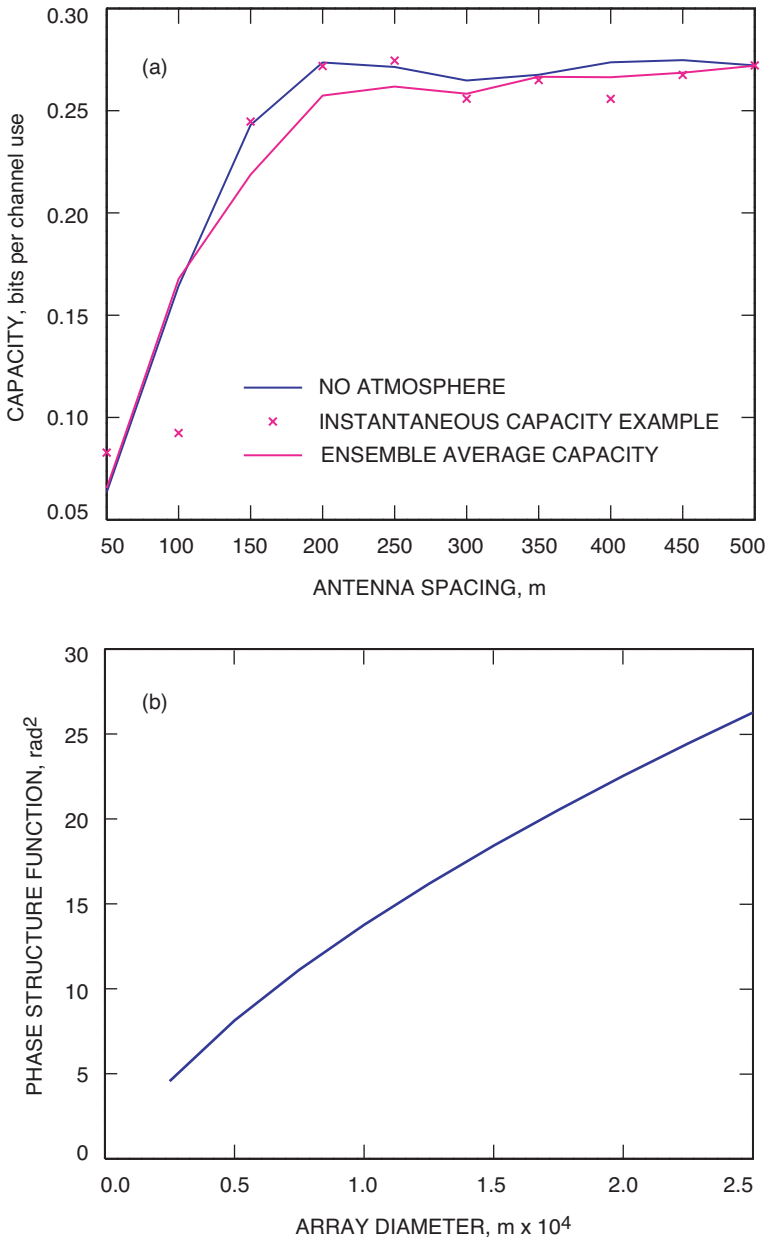

Fig. 11. Using a 50-element linear Ka-band array with the interference source 1 μrad away from the desired signal and 0 dB combined symbol SNR ($P_I = P_S$): (a) capacity as a function of element spacing using spatially correlated atmospheric phase values and (b) values of the phase structure function across the array as a function of array diameter.

References

[1] C. E. Shannon, "A Mathematical Theory of Communication," *The Bell System Technical Journal*, vol. 27, pp. 379–423 and 623–656, July and October 1948.

[2] T. Cover and J. Thomas, *Elements of Information Theory*, New York: Wiley Interscience, 1991.

[3] N. Chiurtu and B. Rimoldi, "Varying the Antenna Locations to Optimize the Capacity of Multi-Antenna Gaussian Channels," *Proceedings of ICASSP 2000*, Istanbul, Turkey, pp. 3121–3123, June 2000.

[4] K.-M. Cheung and V. Vilnrotter, "Channel Capacity of an Array System for Gaussian Channels with Applications to Combining and Noise Cancellation," *The Telecommunications and Data Acquisition Progress Report 42-124, October–December 1995*, Jet Propulsion Laboratory, Pasadena, California, pp. 53–62, February 15 1996. http://ipnpr/progress_report/42-124/124D.pdf

[5] D. Petersen and D. Middleton, "Sampling and Reconstruction of Wave-Number-Limited Functions in n-Dimensional Euclidean Spaces," *Information and Control*, vol. 5, pp. 279–323, 1962.

[6] T. Anderson, *An Introduction to Multivariate Statistical Analysis*, New York: Wiley, 1984.

[7] D. L. Jones, "Geometric Configuration Constraints for Large Deep Space Network Arrays," *The Interplanetary Network Progress Report*, vol. 42-157, Jet Propulsion Laboratory, Pasadena, California, pp. 1–9, May 15, 2004. http://ipnpr/progress_report/42-157/157F.pdf

[8] C. H. Lee, V. Vilnrotter, E. Satorius, Z. Ye, D. Fort, and K.-M. Cheung, "Large-Array Signal Processing for Deep-Space Applications," *The Interplanetary Network Progress Report 42-150, April–June 2002*, Jet Propulsion Laboratory, Pasadena, California, pp. 1–28, August 15, 2002. http://ipnpr/progress_report/42-150/150I.pdf

[9] R. N. Treuhaft and G. E. Lanyi, "The Effect of the Dynamic Wet Troposphere on VLBI Measurements," *The Telecommunications and Data Acquisition Progress Report 42-84, October–December 1985*, Jet Propulsion Laboratory, Pasadena, California, pp. 1–17, February 15, 1986. http://ipnpr/progress_report/42-84/84A.PDF

[10] A. R. Thompson, J. M. Moran, and G. W. Swenson, *Interferometry and Synthesis in Radio Astronomy*, New York: Wiley Interscience, 2001.